PHYSICAL REVIEW D **82,** 036008 (2010)

Precision determination of weak charge of ^{133}Cs from atomic parity violation

S. G. Porsev,[1,2,3] K. Beloy,[1,4] and A. Derevianko[1]

[1]*Physics Department, University of Nevada, Reno, Nevada 89557, USA*
[2]*School of Physics, University of New South Wales, Sydney, New South Wales 2052, Australia*
[3]*Petersburg Nuclear Physics Institute, Gatchina, Leningrad District 188300, Russia*
[4]*Centre for Theoretical Chemistry and Physics, The New Zealand Institute for Advanced Study, Massey University Auckland, Private Bag 102904, 0745, Auckland, New Zealand*

(Received 21 June 2010; published 30 August 2010)

We discuss results of the most accurate to-date test of the low-energy electroweak sector of the standard model of elementary particles. Combining previous measurements with our high-precision calculations we extracted the weak charge of the ^{133}Cs nucleus, $Q_W = -73.16(29)_{\rm exp}(20)_{\rm th}$ [S. G. Porsev, K. Beloy, and A. Derevianko, Phys. Rev. Lett. **102**, 181601 (2009)]. The result is in perfect agreement with $Q_W^{\rm SM}$ predicted by the standard model, $Q_W^{\rm SM} = -73.16(3)$, and confirms energy dependence (or running) of the electroweak interaction and places constraints on a variety of new physics scenarios beyond the standard model. In particular, we increase the lower limit on the masses of extra Z-bosons predicted by models of grand unification and string theories. This paper provides additional details to the earlier paper. We discuss large-scale calculations in the framework of the coupled-cluster method, including full treatment of single, double, and valence triple excitations. To determine the accuracy of the calculations we computed energies, electric-dipole amplitudes, and hyperfine-structure constants. An extensive comparison with high-accuracy experimental data was carried out.

DOI: 10.1103/PhysRevD.82.036008 PACS numbers: 11.30.Er, 31.15.am

I. INTRODUCTION

Atomic parity violation (APV) places powerful constraints on new physics beyond the standard model of elementary particles [1]. The APV measurements are interpreted in terms of the weak nuclear charge Q_W, quantifying the strength of the electroweak coupling between atomic electrons and quarks of the nucleus. At the tree level the weak nuclear charge is given by a simple formula

$$Q_W = -N + Z(1 - 4\sin^2\theta_W), \tag{1}$$

where N is the number of neutrons, Z is the nuclear charge, and θ_W is the Weinberg angle. Since $\sin^2\theta_W$ is close to 0.23, the weak nuclear charge Q_W is numerically close to $-N$.

In Ref. [2] we reported the most accurate to-date determination of this coupling strength by combining previous measurements [3,4] with high-precision calculations in the cesium atom. We found the result $Q_W(^{133}\text{Cs}) = -73.16(29)_{\rm exp}(20)_{\rm th}$ [2] to be in a perfect agreement with $Q_W^{\rm SM}$ predicted by the standard model (SM), $Q_W^{\rm SM} = -73.16(3)$ [5]. In this work we provide a detailed account of the calculation carried out in Ref. [2].

Historically, APV helped to establish the validity of the SM [6–8]. While a number of APV experiments have been carried out [9–15], the most accurate measurement is due to Wieman and collaborators [3]. They determined the ratio of $E_{\rm PNC}/\beta = 1.5935(56)$ mV/cm (where $E_{\rm PNC}$ is the parity nonconserving amplitude defined below by Eq. (2) and β is the vector transition polarizability) on the forbidden $6S_{1/2} \to 7S_{1/2}$ transition in atomic cesium with an accuracy of 0.35%. This measurement does not directly translate into an electroweak observable of the same accuracy, as the interpretation of the experiment requires input from atomic theory, which links Q_W to the signal. Q_W is treated as a parameter and by combining $E_{\rm PNC}$ calculations with measurements, the value of Q_W is extracted and can be compared with the SM value either revealing or constraining new physics.

The parity nonconserving (PNC) amplitude for the $6S_{1/2} \to 7S_{1/2}$ transition in cesium may be evaluated as

$$E_{\rm PNC} = \sum_n \frac{\langle 7S_{1/2}|D_0|nP_{1/2}\rangle\langle nP_{1/2}|H_W|6S_{1/2}\rangle}{E_{6S_{1/2}} - E_{nP_{1/2}}} + \sum_n \frac{\langle 7S_{1/2}|H_W|nP_{1/2}\rangle\langle nP_{1/2}|D_0|6S_{1/2}\rangle}{E_{7S_{1/2}} - E_{nP_{1/2}}}. \tag{2}$$

Here D and H_W are electric-dipole and weak interaction operators, and E_i appearing in the denominators are atomic energy levels. The effective weak interaction mediated by Z-bosons averaged over quarks reads $H_W = -\frac{G_F}{\sqrt{8}} Q_W \gamma_5 \rho(\mathbf{r})$, where G_F is the Fermi constant, γ_5 is the Dirac matrix, and $\rho(\mathbf{r})$ is the neutron-density distribution.

Interpretation of the PNC measurements requires evaluating Eq. (2). Although the underlying theory of quantum electrodynamics (QED) is well established, the atomic many-body problem is intractable. Reaching theoretical accuracy equal to or better than the experimental accuracy of 0.35% has been a challenging task (see Fig. 1). An important 1% accuracy milestone has been reached by

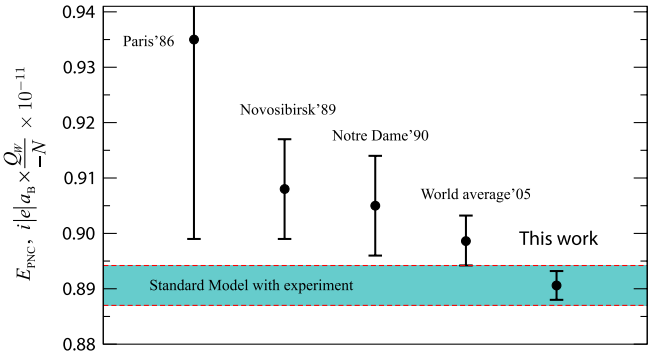

FIG. 1 (color online). Progress in evaluating the PNC amplitude. Points marked Paris '86, Novosibirsk '89, or Notre Dame '90 correspond to Refs. [16,17,64]. The point "World average '05" is due to efforts of several groups [18–22] on sub-1% Breit, QED, and neutron-skin corrections reviewed in Ref. [23]. The strip corresponds to a combination of the standard model Q_W with measurements [3,4]. The edges of the strip correspond to $\pm\sigma$ of the measurement. Here we express $E_{\rm PNC}$ in conventional units of $i|e|a_{\rm B}(-Q_W/N)\times 10^{-11}$, where e is the elementary charge and $a_{\rm B}$ is the Bohr radius. These units factor out a ratio of Q_W to its approximate value, $-N$.

the Novosibirsk [16] and Notre Dame [17] groups in the late 1980s. More recently, several groups have contributed to understanding sub-1% corrections, primarily due to the Breit (magnetic) interaction and radiative QED processes [18–22] (reviewed in [23]). The results of these calculations are summarized by the "World average '05" point of Fig. 1, which has a 0.5% error bar reflecting this progress. As of 2005, the sensitivity to new physics has been limited by the accuracy of solving the basic correlation problem. Here we report important progress in solving it.

We wish to evaluate accurately the sum (2). The cesium atom has one loosely bound valence electron $v = 6s_{1/2}, 6p_{1/2}, \ldots$ outside a closed-shell core $1s^2 2s^2 2p^2_{1/2} \ldots 5d^6_{5/2}$. We compute atomic wave functions, energies, and matrix elements and sum over the intermediate states. We solve the eigenvalue problem $H|\Psi_v\rangle = E_v|\Psi_v\rangle$ and find atomic wave functions and energies. Our specific scheme [23–26] of solving the atomic many-body problem is rooted in the coupled-cluster method [27]. Details will be provided in the next section.

The paper is organized as follows. In Sec. II we describe the coupled-cluster (CC) approximation including single, double, and valence triple excitations and present the results for the low-lying energy levels. In Sec. III we evaluate the hyperfine-structure constants, the matrix elements of the electric-dipole moment, and the PNC amplitude. An analysis of uncertainty of the PNC amplitude is also presented. In Sec. IV we extract the weak nuclear charge from the theoretical and experimental quantities and discuss implications for particle physics. If not stated otherwise atomic units ($\hbar = |e| = m_e = 1$) are used throughout.

II. COUPLED-CLUSTER APPROXIMATION

We employ an approximation rooted in the coupled-cluster method [28,29]. The key difference compared to the previous CC-type calculations for univalent atoms (see, e.g., Refs. [30–35]) is our additional inclusion of valence triple excitations in the expansion of the cluster amplitude. We refer to this approximation as the coupled-cluster single, double, and valence triple (CCSDvT) method. Details of our approximation may be found in Refs. [23–26]. Below we briefly recapitulate its main features and present numerical results.

We choose the lowest-order Hamiltonian to include the relativistic kinetic energy operator of electrons and their interaction with the nucleus and the V^{N-1} (frozen-core) Dirac-Hartree-Fock (DHF) potential. The single-particle orbitals and energies ε_i are found from the set of the frozen-core DHF equations. With the DHF single-particle orbitals, the second-quantized Hamiltonian reads

$$H = H_0 + G = \sum_i \varepsilon_i N[a_i^\dagger a_i] + \frac{1}{2}\sum_{ijkl} g_{ijkl} N[a_i^\dagger a_j^\dagger a_l a_k]. \tag{3}$$

Here H_0 is the one-electron lowest-order Hamiltonian, G is the residual Coulomb interaction, $a_i^\dagger$ and a_i are the creation and annihilation operators, and $N[\cdots]$ is the normal product of operators with respect to the core quasivacuum state $|0_c\rangle$. Indices i, j, k, and l range over all possible single-particle orbitals, and g_{ijkl} are the Coulomb matrix elements.

The exact many-body state $|\Psi_v\rangle$ can be represented as follows:

$$\begin{aligned}|\Psi_v\rangle &= N[\exp(K)]|\Psi_v^{(0)}\rangle \\ &= \left(1 + K + \frac{1}{2!}N[K^2] + \cdots\right)|\Psi_v^{(0)}\rangle,\end{aligned} \tag{4}$$

where $|\Psi_v^{(0)}\rangle$ is the lowest-order DHF state. The cluster operator K is expressed in terms of connected diagrams of the wave operator. In our approach the operator K is approximated by

$K \approx S_c + D_c + S_v + D_v + T_v =$

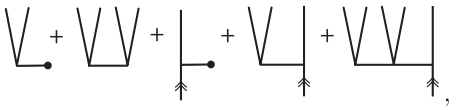 (5)

with the double-headed arrow representing the valence state. Here S_v and D_v (S_c and D_c) are the valence (core) singles and doubles, and T_v are the valence triples. Compared to the core excitations, the valence amplitudes involve excitations of the valence electron. A popular singles-doubles (SD) approximation [30] corresponds to neglecting nonlinear terms in the expansion (4) and valence triples in Eq. (5).

Below we present the topological structure of the equations for valence cluster amplitudes in the CCSDvT approximation. The equations in the coupled-cluster singles-doubles approximation (i.e., without triples) are presented in explicit form in Ref. [36]. A detailed tabulation of the formulas for the valence triple amplitudes is given in Ref. [25]. Since we do not take core triples into consideration, the CCSDvT equations for the core amplitudes S_c and D_c are the same as in [36].

The total energy of the valence electron is given by the sum of the DHF value and the correlation energy, δE_v,

$$E^{\rm tot}_{\rm CCSDvT} = E_{\rm DHF} + \delta E_v. \tag{6}$$

Following the notation of Ref. [26], we can represent the correlation valence energy δE_v as

$$\delta E_v = \delta E_{\rm SD} + \delta E_{\rm CC} + \delta E_{\rm vT}, \tag{7}$$

where the correction $\delta E_{\rm SD}$ is obtained within the SD approach, the correction $\delta E_{\rm CC}$ comes from nonlinear CC contributions, and $\delta E_{\rm vT}$ is due to valence triples.

The topological structure for the valence singles and valence doubles equations may be represented as [26]

$$\begin{aligned} -[H_0, S_v] + \delta E_v S_v \approx {\rm SD} &+ S_v[S_c \otimes S_v] + S_v[S_c \otimes S_c] \\ &+ S_v[S_c \otimes D_v] + S_v[S_v \otimes D_c] \\ &+ S_v[T_v], \end{aligned} \tag{8}$$

$$\begin{aligned} -[H_0, D_v] + \delta E_v D_v \approx {\rm SD} &+ D_v[S_c \otimes S_v] + D_v[S_c \otimes S_c] \\ &+ D_v[S_c \otimes D_v] + D_v[S_v \otimes D_c] \\ &+ D_v[S_c \otimes D_c] + D_v[D_c \otimes D_v] \\ &+ D_v[T_v]. \end{aligned} \tag{9}$$

Here $[H_0, S(D)_v]$ are commutators. $S_v[S_c \otimes S_v]$ stands for a contribution resulting from a product of clusters S_c and S_v. All other terms are defined in a similar fashion. SD terms encapsulate contributions from the SD approximation [30].

For valence triple amplitudes we obtain symbolically

$$-[H_0, T_v] + \delta E_v T_v \approx T_v[D_c] + T_v[D_v]. \tag{10}$$

The contributions $T_v[D_c]$ and $T_v[D_v]$ denote the effect of core and valence doubles on valence triples, respectively. In the present analysis we include only these effects, while omitting the effect of valence triples on valence triples and nonlinear CC contributions [26]. These are higher-order effects that are prohibitively time-consuming for the 55-electron cesium atom.

A numerical solution of the CCSDvT equations provides us with the cluster amplitudes and correlation energies. With the obtained wave functions for two valence states w and v we may evaluate various matrix elements (MEs),

$$Z_{wv} = \frac{\langle \Psi_w | \sum_{ij} \langle i|z|j\rangle a_i^\dagger a_j | \Psi_v \rangle}{\sqrt{\langle \Psi_w|\Psi_w\rangle \langle \Psi_v|\Psi_v\rangle}}. \tag{11}$$

The corresponding CCSDvT expressions are given in Ref. [25]. There are two important modifications compared to the earlier computations [17]: (i) explicit inclusion of valence triples in the expressions for matrix elements and (ii) dressing of lines and vertices in expressions for matrix elements. The dressing mechanism [24] may be explained as follows: when the CC exponent is expanded in Eq. (11), we encounter an infinite number of terms. The resulting series may be partially summed by considering the topological structure of the product of cluster amplitudes, which may be classified using the language of n-body insertions. We include two types of insertions: particle- and hole-line insertions (line ''dressing'') and two-particle and two-hole random-phase-approximation-like insertions.

Our CCSDvT code is an extension of the relativistic SD code [34] which employs a B-spline basis set [37]. Our present version uses a more robust dual-kinetic-balance B-spline basis set [38] as described in Ref. [39]. This basis numerically approximates a complete set of single-particle atomic orbitals. Here, for each partial wave ℓ we use 35 out of $N_{\rm bas} = 40$ positive-energy basis functions generated in a cavity of radius $R_{\rm cav} = 75$ bohr. Basis functions with $\ell_{\rm max} \leq 5$ are used for single and double excitations. For triple excitations we employ a more limited set of basis functions with $\ell_{\rm max}(T_v) \leq 4$. Excitations from core subshells $[4s, \ldots, 5p]$ are included in the calculations of triples while excitations from subshells $[1s, \ldots, 3d]$ are discarded. A basis set extrapolation correction to infinitely large $\ell_{\rm max}$, $N_{\rm bas}$, and $R_{\rm cav}$ is added separately.

Computations were done on a nonuniform grid of 500 points with 15 points inside the nucleus. The nuclear charge distribution was approximated by $\rho(r) = \rho_0/(1 + \exp[(r-c)/a])$ both when solving the DHF equations and evaluating weak interaction matrix elements. For ^{133}Cs, $c = 5.6748$ fm and $a = 0.52338$ fm.

Numerical results for the energies are presented in Table I. The dominant contribution to the energies comes from the DHF values. Correlation corrections ($\delta E_{\rm SD}$, $\delta E_{\rm CC}$, and $\delta E_{\rm vT}$) are dominated by the SD contribution. We also incorporate small complementary corrections due to the Breit interaction, basis extrapolation ($\delta E_{\rm extrap}$), and quantum-electrodynamic (QED) radiative corrections. The agreement between our *ab initio* and experimental values is at the level of 0.3% for the $6S$ state and 0.1–0.2% for all other states (experimental uncertainties are negligible for comparisons at this level).

Since the CCSDvT method is an approximation, we miss certain correlation effects (due to omitted quadruple and higher-rank excitations). This is the cause of the difference between computed and experimental energies in Table I. To partially account for the missing contributions in calculations of matrix elements, we additionally

TABLE I. Contributions to removal energies of $6S_{1/2}$, $6P_{1/2}$, $7S_{1/2}$, and $7P_{1/2}$ states for cesium in cm^{-1} in different approximations. A comparison with experimental values is presented in the bottom panel; experimental uncertainties are negligible at the level displayed.

	$6S_{1/2}$	$6P_{1/2}$	$7S_{1/2}$	$7P_{1/2}$
$E_{\rm DHF}$	27 954	18 790	12 112	9223
$\delta E_{\rm SD}$	3868	1610	827	460
$\delta E_{\rm CC}$	−379	−178	−60	−43
$\delta E_{\rm vT}$	−151	−44	−30	−12
$E^{\rm tot}_{\rm CCSDvT}$	31 292	20 178	12 849	9628
$\delta E_{\rm Breit}$[a]	2.6	−7.1	0.3	−2.5
$\delta E_{\rm QED}$[b]	−17.6	−4.1	−0.4	−0.1
$\delta E_{\rm extrap}$	32.2	15.5	7.1	4.6
$E^{\rm tot}_{\rm final}$	31 309	20 182	12 856	9630
$E_{\rm experim}$[c]	31 406	20 228	12 871	9641

[a]Reference [40];
[b]Reference [41];
[c]Reference [42].

correct the CCSDvT wave functions using a semiempirical procedure suggested in Ref. [43] (see justification in Ref. [26]). In this approach, the valence singles, S_v, are rescaled by the ratio of experimental and theoretical correlation energies. A consistent definition of the experimental correlation energies ($\delta E_v^{\rm exp}$) requires removing the Breit and QED corrections from the experimental energy, i.e.,

$$\delta E_v^{\rm exp} = E_{\rm exp} - E_{\rm DHF} - \delta E_{\rm Breit} - \delta E_{\rm QED}. \qquad (12)$$

We will refer to results obtained using the described procedure as "scaling."

III. EVALUATION OF THE PARITY NONCONSERVING AMPLITUDE AND SUPPORTING QUANTITIES

Below we present details for the evaluation of the parity nonconserving amplitude for the $6S_{1/2} \to 7S_{1/2}$ transition given by Eq. (2). The CCSDvT method is an approximation, and an important part of the entire problem lies with evaluating the theoretical accuracy of the computed PNC amplitude. The PNC amplitude cannot be directly compared to an experimental measurement. As seen from Eq. (2), one needs to know the matrix elements of the electric-dipole operator, the energies, and the matrix elements of the weak interaction H_W. The quality of calculations of the dipole transition amplitudes and energy levels can be established by comparing them with experimental data, while for the matrix elements of the weak interaction such a direct comparison is not possible. Instead, we may consider the operator of the hyperfine interaction. Matrix elements of both the hyperfine and weak interaction are accumulated near the origin. Therefore, calculating hyperfine-structure (HFS) constants for the low-lying states and comparing them with the experimental data allows us to assess the quality of the constructed wave functions near the nucleus.

The results of calculations of the HFS constants and dipole matrix elements between the low-lying states are

TABLE II. Magnetic-dipole hyperfine-structure constants A (in MHz) for ^{133}Cs. Results of calculations and comparison with experimental values are presented. See text for the explanation of entries.

	$A(6S_{1/2})$	$A(6P_{1/2})$	$A(7S_{1/2})$	$A(7P_{1/2})$
DHF	1424.9	160.90	391.53	57.61
SD	2436.7	310.73	560.85	98.34
Δ (CC)	−110.1	−22.40	−13.43	−5.26
Δ (vT)	−29.6	2.35	−1.92	1.18
Δ (scaling)	14.7	2.59	0.38	0.41
Complementary corrections:				
Line and vertex dressing	−9.4	−1.92	−1.22	−0.53
Breit[a]	4.9	−0.52	1.15	−0.15
QED	−9.7[b]	−0.05[c]	−2.30[d]	−0.02[d]
Basis extrapolation	9.1	0.71	1.08	0.10
Final results	2306.6	291.49	544.59	94.07
Experiment	2298.16	291.9135(15)[e] 291.9309(12)[h]	545.90(9)[f]	94.35(4)[g]
Difference	0.36%	−0.15%	−0.24%	−0.30%

[a]Reference [40];
[b]Reference [44];
[c]Reference [45];
[d]The QED corrections for the $7S_{1/2}$ and $7P_{1/2}$ states were obtained by scaling those for the $6S_{1/2}$ and $6P_{1/2}$ states;
[e]Reference [46];
[f]References [47];
[g]Reference [48];
[h]Reference [49].

TABLE III. Reduced matrix elements of the electric-dipole moment operator D (in atomic units [a.u.]) for ^{133}Cs. Results of calculations and comparisons with experimental values are presented. See text for the explanation of entries.

	$\lvert\langle 6P_{1/2}\rVert D\rVert 6S_{1/2}\rangle\rvert$	$\lvert\langle 7P_{1/2}\rVert D\rVert 6S_{1/2}\rangle\rvert$	$\lvert\langle 6P_{1/2}\rVert D\rVert 7S_{1/2}\rangle\rvert$	$\lvert\langle 7P_{1/2}\rVert D\rVert 7S_{1/2}\rangle\rvert$
DHF	5.2777	0.3717	4.4131	11.009
SD	4.4831	0.2969	4.1984	10.256
Δ (CC)	0.0717	0.0058	0.0528	0.045
Δ (vT)	−0.0423	−0.0302	0.0038	0.009
Δ (scaling)	−0.0123	0.0033	−0.0138	−0.010
Complementary corrections:				
Line and vertex dressing	0.0036	0.0016	−0.0004	0.001
Breit[a]	−0.0010	0.0019	0.0049	−0.003
QED	0.0027[b,c]	−0.0028[c]	−0.0043[c]	0.005[c]
Basis extrapolation	0.0038	0.0005	0.0036	0.005
Final result	4.5093	0.2769	4.2450	10.307
Experiment	4.5097(45)[d]	0.2825(20)[e]	4.233(22)[f]	10.308(15)[g]
	4.4890(65)[h]	0.2757(20)[i]		
Other results	4.5064(47)[j]			

[a]Reference [40];
[b]Reference [50];
[c]Reference [41];
[d]Reference [51];
[e]Reference [52] (as reevaluated in Ref. [53]);
[f]Reference [54];
[g]Reference [55];
[h]Reference [56];
[i]Reference [53];
[j]Reference [57].

presented in Tables II and III. For the HFS calculations we assumed a uniform distribution of the nuclear magnetization (magnetization radius of 5.6748 fm) and used the nuclear g-factor of 0.737 72. We explicitly list DHF and SD values. The entry Δ (CC) indicates the change in the value caused by including the nonlinear terms in the equations for core and valence singles and doubles. Likewise, Δ (vT) and Δ (scaling) arise due to a subsequent addition of valence triples and scaling. We also incorporated smaller corrections: line and vertex dressing (discussed in detail in [24]), the Breit interaction, the QED corrections, and the corrections due to the basis set extrapolation. In the lower panels of the tables we compare our theoretical results with the most accurate experimental results. We find that the discrepancies between theoretical and experimental values for the HFS constants are 0.15–0.35% (experimental uncertainties for HFS constants being well below this level). For dipole matrix elements the theoretical values are within the error bars of the experiments. The uncertainty estimate of E_{PNC} can be carried out using geometric means $\sqrt{A_{nS_{1/2}}A_{n'P_{1/2}}}$ [58], as the relative uncertainty of this combination mimics the relative uncertainty of the ME of the weak interaction $\langle nS_{1/2}|H_W|n'P_{1/2}\rangle$. Deviations of these combinations from experimental data are shown in the upper panel of Fig. 2. We find that the standard deviation of our theoretical values for these combinations from the experimental values is 0.2%.

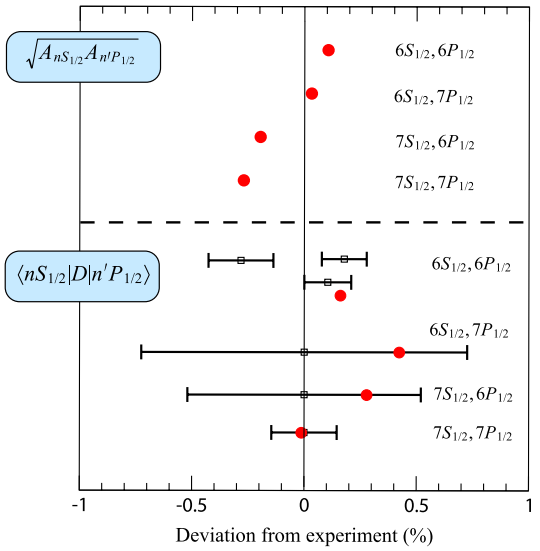

FIG. 2 (color online). Deviations of computed values (red filled circles) from experimental data (centered at zero). The upper panel displays combinations of magnetic hyperfine-structure constants $\sqrt{A_{nS_{1/2}}A_{n'P_{1/2}}}$ which mimic matrix elements of the weak interaction. For these combinations, experimental error bars are negligible compared to the theoretical accuracy. The lower panel exhibits deviations of the computed dipole matrix elements from the most accurate experimental results [53,65].

Now we proceed to evaluate the PNC amplitude (2) by directly summing over the intermediate $nP_{1/2}$ ($n = 6$–9) states [17]. These states contribute 99% to the final $E_{\rm PNC}$ value. In Table IV we present the matrix elements of the electric-dipole operator and H_W, as well as the energy differences. Contributions from the 6–$9P_{1/2}$ states to $E_{\rm PNC}$ are also listed. The matrix elements were computed in the CCSDvT approximation with dressing. We also used the scaling procedure. Energy differences were based on the experimental energies with the Breit and QED corrections removed. For the $6S_{1/2}$, $6P_{1/2}$, $7S_{1/2}$, and $7P_{1/2}$ states we used the following "corrected" energies:

$$E_{\rm corr} = E_{\rm exp} - \delta E_{\rm Breit} - \delta E_{\rm QED}. \tag{13}$$

The contribution of the higher-energy intermediate $8P_{1/2}$ and $9P_{1/2}$ states to the PNC amplitude is suppressed; for these states we used the full experimental energies.

The results for the PNC amplitude are presented in Table V. Each subsequent line in the upper panel of the table corresponds to an increasingly more complex approximation. We start from the SD approximation. Inclusion of nonlinear CC terms ("CC" entry) modifies the SD result by almost 2%. At the next step we incorporate valence triples. Because of the importance of these terms we present a detailed breakdown of the associated effects. We distinguish between indirect and direct contributions from the valence triples. Indirect effects of triples come from modifying energies and single and double excitations through the Schrödinger equation. In Table V the relevant values are marked with "no vT in MEs." The direct contribution arises from explicit presence of valence triples (vT) in expressions for the MEs. We also list the results obtained without scaling ["vT (no vT in MEs; pure)"] and including it ["vT (no vT in MEs; scaled)"]. We find that the PNC amplitude is insensitive to scaling. Note that a

TABLE V. Contributions to $E_{\rm PNC}$ in different approximations. $E_{\rm PNC}$ and Δ are in units of $i|e|a_{\rm B}(-Q_W/N) \times 10^{-11}$, where $N = 78$ is the number of neutrons in ^{133}Cs nucleus. In the upper panel of the table Δ is the difference between the results given in this row and the previous row. In the lower panels Δ determines the respective contribution to $E_{\rm PNC}$. Assessment of the theoretical uncertainty is described in the text.

Approximation	$E_{\rm PNC}$	Δ
"Main" term:		
SD	0.8952	
CC	0.8800	−0.0152
vT (no vT in MEs; pure)	0.8911	0.0111
vT (no vT in MEs; scaled)	0.8915	0.0004
vT (no vT in MEs; scaled, $E_{\rm corr}$)	0.8885	−0.0030
vT (scaled, $E_{\rm corr}$)	0.8856	−0.0029
Line-dressing	0.8825	−0.0031
Vertex dressing	0.8823	−0.0002
Final main ($n = 6$–9)	0.8823(17)	
Tail:		
$n \geq 10$		0.0195
Core contribution		−0.0020
Basis extrapolation		−0.000 06
Total	0.8998(24)	
Complementary corrections:		
Breit[a]		−0.0054
QED[b]		−0.0024
Neutron skin [c]		−0.0017
e-e weak interaction[d]		0.0003
Sum of corrections		−0.0092
Final $E_{\rm PNC}$	0.8906(24)	

[a]Reference [40];
[b]Reference [22];
[c]Reference [19];
[d]References [21,59].

TABLE IV. Contribution to $E_{\rm PNC}$ from intermediate states 6–$9P_{1/2}$. Dipole matrix elements are of the form $\langle nLJ; m_J = 1/2|D_z|n'L'J'; m_{J'} = 1/2\rangle$. Assessment of the theoretical uncertainty is described in the text.

		$6S_{1/2}$ perturbed		
n	$\langle 7S_{1/2}\|D\|nP_{1/2}\rangle$ a.u.	$\langle nP_{1/2}\|H_W\|6S_{1/2}\rangle$ $10^{-11}i(-Q_W/N)$ a.u.	$E_{6S_{1/2}} - E_{nP_{1/2}}$ a.u.	Contribution $10^{-11}i(-Q_W/N)$ a.u.
6	1.7327	0.055 75	−0.050 949	−1.8962
7	4.2071	−0.031 69	−0.099 227	1.3435
8	0.3769	−0.021 18	−0.117 208	0.0681
9	0.1423	−0.016 05	−0.125 993	0.0181
		$7S_{1/2}$ perturbed		
n	$\langle nP_{1/2}\|D\|6S_{1/2}\rangle$ a.u.	$\langle 7S_{1/2}\|H_W\|nP_{1/2}\rangle$ $10^{-11}i(-Q_W/N)$ a.u.	$E_{7S_{1/2}} - E_{nP_{1/2}}$ a.u.	Contribution $10^{-11}i(-Q_W/N)$ a.u.
6	−1.8402	−0.026 97	0.033 573	1.4783
7	0.1134	0.01525	−0.014 705	−0.1176
8	0.0305	0.010 24	−0.032 686	−0.0096
9	0.0128	0.007 76	−0.041 471	−0.0024
Total				0.8823(17)

similar conclusion was drawn in Ref. [58]. As the next step we replace the calculated energies in the denominators of Eq. (2) by the experimental energies $E_{\rm corr}$ as explained above. The resulting entries include the $E_{\rm corr}$ qualifier. We also include line and vertex dressing; the resulting matrix elements and detailed breakdown of results are listed in Table IV. We also add contributions of intermediate states above $9P_{1/2}$, including continuum, and contributions from core excitations. These contributions are denoted as "$n \geq 10$" and "Core contribution," respectively. Finally, the lower panel summarizes well-established non-Coulomb contributions such as the magnetic interaction between the electrons (Breit), radiative (QED), and other smaller corrections.

The accuracy of the PNC amplitude was estimated by comparing theoretical results for energies, dipole matrix elements, and magnetic hyperfine constants with high-precision experimental data (see Tables I, II, and III). We find that the experimental energies are reproduced with an accuracy of 0.1–0.3%. Relevant dipole matrix elements are within the error bars of the experiments. Finally, since the hyperfine constants A are accumulated in the nuclear region, matrix elements of the weak interaction $\langle nS_{1/2}|H_W|n'P_{1/2}\rangle$ may be tested by forming the geometric mean $\sqrt{A_{nS_{1/2}}A_{n'P_{1/2}}}$; see Ref. [58]. We find that the standard deviation of theoretical values from experiment is 0.2%. As a test of stability of the final result, we also computed the main term using *ab initio* (i.e., without scaling) CCSDvT matrix elements and energies. The result, 0.8839, deviates by 0.18% from our scaled value of 0.8823 in Table V. Based on these tests, we assign an error of 0.2% to the main term. Finally, the "tail" lumps contributions of remaining excited $nP_{1/2}$ states (including continuum) and core-excited states. The tail was computed using a blend of many-body approximations and we assign a 10% uncertainty to this contribution based on the spread of its value in different approximations. The final result includes smaller non-Coulomb corrections and its uncertainty was estimated by adding individual uncertainties in quadrature.

Our uncertainty in $E_{\rm PNC}$ represents a two-fold improvement over calculations [58] and a four-fold improvement over Ref. [17]. Both calculations report a value of 0.908 for the total Coulomb-correlated value, larger by 0.9% than our 0.27%-accurate result. The reason for the shift in our more complete calculations is three-fold: (i) direct contributions of the triple excitations to matrix elements (0.3%), (ii) line-dressing of diagrams for matrix elements (0.3%), and (iii) consistent removal of Breit and QED corrections from experimental energies used in the scaling procedure (0.3%). Representative diagrams are shown in Fig. 3.

As discussed, we make a distinction between the indirect and direct contributions of T_v to matrix elements [25]. Indirect effects of triples come from modifying energies and single and double excitations. In the previous work

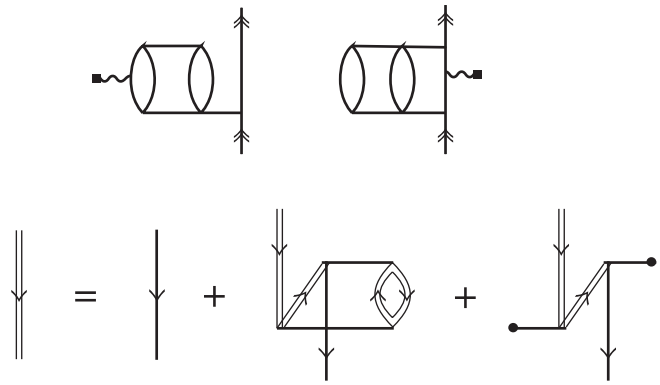

FIG. 3. Many-body diagrams responsible for the shift of the PNC amplitude compared to previous calculations. Top row: sample direct contributions of valence triples to matrix elements (wavy capped line) [25]. Bottom row: iterative equation for line-dressing of the hole line in expressions for matrix elements [24] (similar equation holds for particle lines; exchange diagrams are not shown).

[17,58] it was approximately accounted for by a semi-empirical scaling of single valence excitation (or Brueckner orbitals) to the ratio of the theoretical to experimental correlation energies. Direct T_v contributions to matrix elements, however, cannot be reproduced by the scaling and, moreover, require storing triples; due to large-memory requirements this was not done in Ref. [17,58]. The size of the effect, -0.0029, is given by the difference between entries "vT (no vT in MEs; scaled, $E_{\rm corr}$)" and "vT (scaled, $E_{\rm corr}$)" in Table V. The line-dressing [24] was also not attempted previously. The line-dressing comes from resumming nonlinear contributions to wave functions, Eq. (4), in expressions for matrix elements. A structure of the all-order equations for the dressed hole lines is presented in Fig. 3. The value of the line-dressing correction, -0.0031, is listed in Table V. The direct T_v contributions are most pronounced for the $6S_{1/2} - 7P_{1/2}$ dipole amplitude, where they shift the value by 3%; their omission leads to a 4σ deviation from experiment [53]. Similarly, discarding line-dressing shifts the theoretical values of $A_{6P_{1/2}}$ by 0.8%.

IV. WEAK NUCLEAR CHARGE AND IMPLICATIONS FOR PARTICLE PHYSICS

With the computed $E_{\rm PNC}$ we proceed to extract the electroweak observable. The experiment [3] determined the ratio of $E_{\rm PNC}/\beta = 1.5935(56)$ mV/cm. The most accurate β comes from a combined determination [4,58], $\beta = -26.957(51)a_B^3$. As a result we arrive at the nuclear weak charge

$$Q_W(^{133}\mathrm{Cs}) = -73.16(29)_{\rm exp}(20)_{\rm th}, \qquad (14)$$

where the first uncertainty is experimental and the second uncertainty is theoretical. Taking a weighted average,

$\beta = -26.99(50)a_B^3$, of two determinations [4,53] results in $Q_W(^{133}\mathrm{Cs}) = -73.25(29)_{\mathrm{exp}}(20)_{\mathrm{th}}$. Both values are in a perfect agreement with the prediction of the standard model, $Q_W^{\mathrm{SM}} = -73.16(3)$ of Ref. [5].

While our result is consistent with the SM, it plays a unique and at the same time complementary role to high-energy physics experiments. Our result (i) confirms energy dependence (or running) of the electroweak interaction and (ii) places constraints on a variety of new physics scenarios beyond the standard model.

In physics, the vacuum is never still. Each particle carries a cloud of continuously sprouting virtual particle-antiparticle pairs. The strength of the mutual interaction between two particles becomes dependent on their relative collision energy: at higher energies, the collision partners tend to penetrate deeper inside the shielding clouds. According to the SM, the interaction strength at low energies differs by about 3% from its value at 100 GeV; see Fig. 4. For low energies, where the shielding clouds are penetrated the least, previous analyses [22,23] were consistent with no running. Here we improve the accuracy of probing these least energetic electroweak interactions.

Compared to conventional particle-physics experiments, our result provides a reference point for the least energetic electroweak interactions. With our weak charge, we find the effective interaction strength, $\sin^2\theta_W^{\mathrm{eff}}(E \to 0) = 0.2382(11)$. The result is in agreement with the SM value [60] of 0.2381(6). While an earlier evidence for running of $\sin^2\theta_W$ has been obtained in the parity violating electron-scattering experiment at SLAC [61], the prediction of the SM was outside their experimental error bars. Our work provides a higher-confidence confirmation of the predicted running of the electroweak coupling at low energies.

Notice that the relevant momentum transfer for ^{133}Cs atom is just ~30 MeV [21], but the exquisite accuracy of the interpretation probes minute contributions of the sea of virtual (including so-far undiscovered) particles at a much higher mass scale. The new physics brought by the virtual sea is phenomenologically described by weak isospin-conserving S and isospin-breaking T parameters [62]: $Q_W - Q_W^{\mathrm{SM}} = -0.800S - 0.007T$. At the 1σ level, our result implies $|S| < 0.45$. The parameter S is important, for example, in indirectly constraining the mass of the Higgs particle [62]. Similarly, the extra Z-boson, Z'_χ, discussed in Ref. [2], would lead to a deviation [1] $Q_W - Q_W^{\mathrm{SM}} \approx 84(M_W/M_{Z'_\chi})^2$. We find $M_{Z'_\chi} > 1.4\ \mathrm{TeV}/c^2$, improving the present lower bound on the Z' mass from direct collider searches [63].

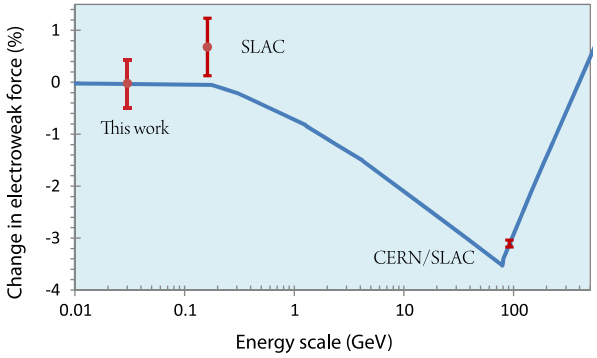

FIG. 4 (color online). Running of the electroweak force. The strength of the electroweak coupling varies depending on the energy scale probed by an experiment. The plot shows the amount of variation relative to the strength at zero energies. The solid line is the prediction [66] of the SM. High-energy experiments at CERN and SLAC have measured the strength of electroweak force at 91 GeV with an accuracy of ~0.1%. In 2005, a SLAC electron-scattering experiment [61] had determined the strength at 0.2 GeV with an accuracy of about 0.5%. Our analysis of atomic parity violation probes the least energetic (30 MeV) electroweak interactions measured so far and the result is in perfect agreement with the SM. Overall, the predicted running of the electroweak force is confirmed over an energy range spanning 4 orders of magnitude.

ACKNOWLEDGMENTS

We thank O. Sushkov, M. Kozlov, J. Erler, W. Marciano, and M. Ramsey-Mussolf for discussions. This work was initiated with support from the NIST precision measurement grant program and supported in part by the NSF.

[1] W. J. Marciano and J. L. Rosner, Phys. Rev. Lett. **65**, 2963 (1990); **68**, 898 (1992).
[2] S. G. Porsev, K. Beloy, and A. Derevianko, Phys. Rev. Lett. **102**, 181601 (2009).
[3] C. S. Wood, S. C. Bennett, D. Cho, B. P. Masterson, J. L. Roberts, C. E. Tanner, and C. E. Wieman, Science **275**, 1759 (1997).
[4] S. C. Bennett and C. E. Wieman, Phys. Rev. Lett. **82**, 2484 (1999).
[5] C. Amsler *et al.*, Phys. Lett. B **667**, 1 (2008).
[6] I. B. Khriplovich, *Parity Non-Conservation in Atomic Phenomena* (Gordon and Breach, New York, 1991).
[7] M.-A. Bouchiat and C. Bouchiat, Rep. Prog. Phys. **60**, 1351 (1997).
[8] J. S. M. Ginges and V. V. Flambaum, Phys. Rep. **397**, 63 (2004).
[9] N. H. Edwards, S. J. Phipp, P. E. G. Baird, and S. Nakayama, Phys. Rev. Lett. **74**, 2654 (1995).
[10] P. A. Vetter, D. M. Meekhof, P. K. Majumder, S. K. Lamoreaux, and E. N. Fortson, Phys. Rev. Lett. **74**, 2658

(1995).
[11] D. M. Meekhof, P. A. Vetter, P. K. Majumder, S. K. Lamoreaux, and E. N. Fortson, Phys. Rev. A **52**, 1895 (1995).
[12] S. J. Phipp, N. H. Edwards, P. E. G. Baird, and S. Nakayama, J. Phys. B **29**, 1861 (1996).
[13] M. J. D. Macpherson, K. P. Zetie, R. B. Warrington, D. N. Stacey, and J. P. Hoare, Phys. Rev. Lett. **67**, 2784 (1991).
[14] K. Tsigutkin, D. Dounas-Frazer, A. Family, J. E. Stalnaker, V. V. Yashchuk, and D. Budker, Phys. Rev. Lett. **103**, 071601 (2009).
[15] K. Tsigutkin, D. Dounas-Frazer, A. Family, J. E. Stalnaker, V. V. Yashchuk, and D. Budker, Phys. Rev. A **81**, 032114 (2010).
[16] V. A. Dzuba, V. V. Flambaum, and O. Sushkov, Phys. Lett. A **140**, 493 (1989).
[17] S. A. Blundell, W. R. Johnson, and J. Sapirstein, Phys. Rev. Lett. **65**, 1411 (1990).
[18] A. Derevianko, Phys. Rev. Lett. **85**, 1618 (2000).
[19] A. Derevianko, Phys. Rev. A **65**, 012106 (2001).
[20] O. P. Sushkov, Phys. Rev. A **63**, 042504 (2001); V. A. Dzuba *et al.*, Phys. Rev. A **63**, 044103 (2001); M. G. Kozlov and S. G. Porsev, Phys. Rev. Lett. **86**, 3260 (2001); W. R. Johnson *et al.*, Phys. Rev. Lett. **87**, 233001 (2001); M. Yu. Kuchiev and V. V. Flambaum, Phys. Rev. Lett. **89**, 283002 (2002); J. Sapirstein *et al.*, Phys. Rev. A **67**, 052110 (2003); A. I. Milstein *et al.*, Phys. Rev. A **67**, 062103 (2003).
[21] A. I. Milstein, O. P. Sushkov, and I. S. Terekhov, Phys. Rev. Lett. **89**, 283003 (2002).
[22] V. M. Shabaev, K. Pachucki, I. I. Tupitsyn, and V. A. Yerokhin, Phys. Rev. Lett. **94**, 213002 (2005).
[23] A. Derevianko and S. G. Porsev, Eur. Phys. J. A **32**, 517 (2007).
[24] A. Derevianko and S. G. Porsev, Phys. Rev. A **71**, 032509 (2005).
[25] S. G. Porsev and A. Derevianko, Phys. Rev. A **73**, 012501 (2006).
[26] A. Derevianko, S. G. Porsev, and K. Beloy, Phys. Rev. A **78**, 010503(R) (2008).
[27] I. Lindgren and J. Morrison, *Atomic Many-Body Theory* (Springer-Verlag, Berlin, 1986), 2nd ed..
[28] F. Coester and H. G. Kümmel, Nucl. Phys. **17**, 477 (1960).
[29] J. Čížek, J. Chem. Phys. **45**, 4256 (1966).
[30] S. A. Blundell, W. R. Johnson, Z. W. Liu, and J. Sapirstein, Phys. Rev. A **40**, 2233 (1989).
[31] S. A. Blundell, W. R. Johnson, and J. Sapirstein, Phys. Rev. A **43**, 3407 (1991).
[32] E. Eliav, U. Kaldor, and Y. Ishikawa, Phys. Rev. A **50**, 1121 (1994).
[33] E. N. Avgoustoglou and D. R. Beck, Phys. Rev. A **57**, 4286 (1998).
[34] M. S. Safronova, A. Derevianko, and W. R. Johnson, Phys. Rev. A **58**, 1016 (1998).
[35] M. S. Safronova, W. R. Johnson, and A. Derevianko, Phys. Rev. A **60**, 4476 (1999).
[36] R. Pal, M. S. Safronova, W. R. Johnson, A. Derevianko, and S. G. Porsev, Phys. Rev. A **75**, 042515 (2007).
[37] W. R. Johnson, S. A. Blundell, and J. Sapirstein, Phys. Rev. A **37**, 307 (1988).
[38] V. M. Shabaev, I. I. Tupitsyn, V. A. Yerokhin, G. Plunien, and G. Soff, Phys. Rev. Lett. **93**, 130405 (2004).
[39] K. Beloy and A. Derevianko, Comput. Phys. Commun. **179**, 310 (2008).
[40] A. Derevianko, Phys. Rev. A **65**, 012106 (2001).
[41] V. V. Flambaum and J. S. M. Ginges, Phys. Rev. A **72**, 052115 (2005).
[42] C. E. Moore, *Atomic Energy Levels* (National Bureau of Standards, Washington, DC, 1958), Vol. III.
[43] S. A. Blundell, J. Sapirstein, and W. R. Johnson, Phys. Rev. D **45**, 1602 (1992).
[44] J. Sapirstein and K. T. Cheng, Phys. Rev. A **67**, 022512 (2003).
[45] J. Sapirstein and K. T. Cheng, Phys. Rev. A **74**, 042513 (2006).
[46] D. Das and V. Natarajan, J. Phys. B **41**, 035001 (2008).
[47] S. L. Gilbert, R. N. Watts, and C. E. Wieman, Phys. Rev. A **27**, 581 (1983).
[48] D. Feiertag, A. Sahm, and G. zu Putlitz, Z. Phys. D **255**, 93 (1972).
[49] V. Gerginov, K. Calkins, C. E. Tanner, J. J. McFerran, S. Diddams, A. Bartels, and L. Hollberg, Phys. Rev. A **73**, 032504 (2006).
[50] J. Sapirstein and K. T. Cheng, Phys. Rev. A **71**, 022503 (2005).
[51] L. Young, W. T. S. J. Hill, S. J. Sibener, S. D. Price, C. E. Tanner, C. E. Wieman, and S. R. Leone, Phys. Rev. A **50**, 2174 (1994).
[52] L. N. Shabanova, Y. N. Monakov, and A. N. Khlyustalov, Opt. Spektrosk. **47**, 3 (1979) [Opt. Spectrosc. (USSR) **47**, 1 (1979)].
[53] A. A. Vasilyev, I. M. Savukov, M. S. Safronova, and H. G. Berry, Phys. Rev. A **66**, 020101 (2002).
[54] M.-A. Bouchiat, J. Guéna, and L. Pottier, J. Phys. (Paris), Lett. **45**, 523 (1984).
[55] S. C. Bennett, J. L. Roberts, and C. E. Wieman, Phys. Rev. A **59**, R16 (1999).
[56] R. J. Rafac, C. E. Tanner, A. E. Livingston, and H. G. Berry, Phys. Rev. A **60**, 3648 (1999).
[57] A. Derevianko and S. G. Porsev, Phys. Rev. A **65**, 052115 (2002).
[58] V. A. Dzuba, V. V. Flambaum, and J. S. M. Ginges, Phys. Rev. D **66**, 076013 (2002).
[59] A. I. Milstein, O. P. Sushkov, and I. S. Terekhov, Phys. Rev. A **67**, 062103 (2003).
[60] A. Czarnecki and W. J. Marciano, Int. J. Mod. Phys. A **15**, 2365 (2000).
[61] P. L. Anthony, R. G. Arnold, C. Arroyo, K. Bega, J. Biesiada, P. E. Bosted, G. Bower, J. Cahoon, R. Carr, G. D. Cates *et al.*, Phys. Rev. Lett. **95**, 081601 (2005).
[62] J. L. Rosner, Phys. Rev. D **65**, 073026 (2002).
[63] T. Aaltonen *et al.*, Phys. Rev. Lett. **99**, 171802 (2007).
[64] C. Bouchiat and C. A. Piketty, Europhys. Lett. **2**, 511 (1986).
[65] L. Young *et al.*, Phys. Rev. A **50**, 2174 (1994); R. J. Rafac *et al.*, Phys. Rev. A **60**, 3648 (1999); A. Derevianko and S. G. Porsev, Phys. Rev. A **65**, 053403 (2002); M.-A. Bouchiat *et al.*, J. Phys. (Paris), Lett. **45**, 523 (1984); S. C. Bennett *et al.*, Phys. Rev. A **59**, R16 (1999).
[66] J. Erler and M. J. Ramsey-Musolf, Phys. Rev. D **72**, 073003 (2005).